

Monitoring pH and whey protein digestion by TD-NMR and MRI in a novel semi-dynamic *in vitro* gastric simulator (MR-GAS)

Ruoxuan Deng^{a,b,*}, Aurimas Seimys^b, Monica Mars^a, Anja E.M. Janssen^b, Paul A.M. Smeets^a

^a Division of Human Nutrition and Health, Wageningen University, Wageningen, the Netherlands

^b Laboratory of Food Process Engineering, Wageningen University & Research, Wageningen, the Netherlands

ARTICLE INFO

Keywords:

Digestion
Nuclear magnetic resonance
Magnetic resonance imaging
Whey protein
Transverse relaxation rate
Longitudinal relaxation rate

ABSTRACT

Gastric digestion is crucial for protein breakdown. Magnetic resonance techniques have a great deal of potential but remain underexplored with regard to their application in the study of food digestion via MRI-markers, such as transverse (R_2) and longitudinal (R_1) relaxation rates. R_2 has been used to monitor gastric digestion of whey protein gels, but only in a static *in vitro* model. It is essential to investigate whether relaxation rates can be valid measures of digestion under dynamic circumstances. We developed a novel MRI-compatible semi-dynamic gastric simulator (MR-GAS) that includes controlled gastric secretion, emptying and mixing at body temperature. PH and protein hydrolysis were measured during protein gel digestion in the MR-GAS. R_2 and R_1 of the supernatant were measured by time-domain nuclear magnetic resonance (TD-NMR). The stomach chamber of the MR-GAS was also scanned with MRI to measure R_2 and R_1 . For TD-NMR, 99% of the variance in R_2 and 96% of variance in R_1 could be explained as a function of protein concentration and $[H^+]$. For MRI, the explained variances were 99% for R_2 and 60% for R_1 . From these analysis, the obtained equations enabled the prediction of protein concentration and pH by R_2 and R_1 . The normalised root mean squared deviation of the predictions for protein concentration were 0.15 (NMR) and 0.18 (MRI), and for pH were 0.12 (NMR) and 0.29 (MRI). In conclusion, the MR-GAS model may be used in a clinical MRI to monitor gastric digestion under *in vitro* dynamic circumstances, by measuring R_2 and R_1 . These results underscore the potential of MRI to monitor nutrients hydrolysis and pH changes in future *in vivo* studies.

1. Introduction

Gastric digestion is a complex dynamic process. It is essential for the breakdown of food matrices, especially those found in protein-rich solid foods. Ingestion of food stimulates the secretion of gastric fluid, which contains pepsin and gastric acid (Singh & Gallier, 2014). Food particles are broken down by mechanical and enzymatic digestion, and the resulting chyme is emptied through the pylorus into the small intestine (Bornhorst, 2017). For dietary proteins, the enzymatic digestion in the stomach by pepsin is especially important since it affects their subsequent digestion and absorption (Bordoni et al., 2011).

In recent years, researchers have developed multiple *in vitro* digestion models and approaches to study gastric digestion (Gouseti, Bornhorst, Bakalis, & Mackie, 2019). These models are useful for studying the molecular mechanisms behind protein breakdown, and have the advantage of well-controlled and reproducible conditions and easy sampling (Brodkorb et al., 2019; Kong & Singh, 2008; Minekus et al.,

2014). However, an *in vitro* model cannot entirely simulate realistic gastrointestinal conditions since *in vivo* digestion comprises a diverse and interconnected set of processes and feedback mechanisms. Moreover, many *in vitro* measurements and conditions cannot be applied *in vivo* due to practical limitations and ethical concerns (Bordoni et al., 2011). This creates a challenge for the verification of *in vitro* results with *in vivo* studies. Therefore, it is important to explore non-invasive approaches feasible for monitoring both *in vitro* and *in vivo* digestion.

Magnetic resonance imaging (MRI) has great potential as a non-invasive approach for examining gastric digestion *in vivo*, not only because it can be used to assess gastric process at a macroscopic level (e.g. gastric emptying), but also because it can be used to study intraluminal processes on a molecular level (Marciani, 2011; Smeets et al., 2020; Spiller & Marciani, 2019). Additionally, time-domain nuclear magnetic resonance (TD-NMR), which has the same underlying principles as MRI, can provide extra information and aid the interpretation of *in vitro* and *in vivo* measurements with MRI, even though NMR is limited

* Corresponding author. Division of Human Nutrition and Health, Wageningen University, Wageningen, the Netherlands.

E-mail address: ruoxuan.deng@wur.nl (R. Deng).

<https://doi.org/10.1016/j.foodhyd.2021.107393>

Received 27 August 2021; Received in revised form 3 November 2021; Accepted 22 November 2021

Available online 26 November 2021

0268-005X/© 2021 The Authors.

Published by Elsevier Ltd.

This is an open access article under the CC BY-NC-ND license

(<http://creativecommons.org/licenses/by-nc-nd/4.0/>).

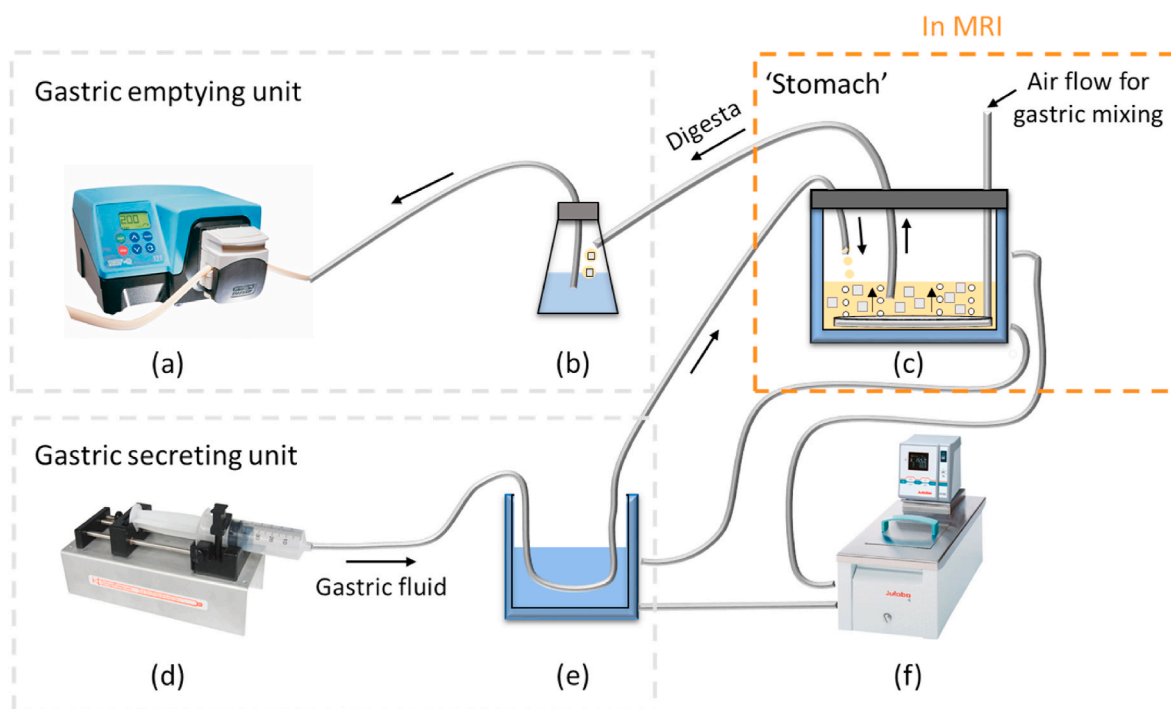


Fig. 1. MRI semi-dynamic compatible gastric simulator (MR-GAS), consisting of a peristaltic pump (a), a sealed vessel with water (b), a water-jacketed ‘stomach’ chamber (c), a syringe pump (d), a container with water to preheat SGF (e), a circulating heater (f).

to *in vitro* measurements (Deng, Janssen, et al., 2020).

Transverse relaxation time (T_2) or rate ($R_2 = T_2^{-1}$) and longitudinal relaxation time (T_1) or rate ($R_1 = T_1^{-1}$) can be measured with both NMR and MRI. R_2 and R_1 reflect how protons in a magnetic field relax back to their equilibrium position after excitation by a radiofrequency pulse. R_2 refers to the spin-spin relaxation in the x-y plane, and R_1 refers to the relaxation of the net magnetisation to realign itself with the direction of the external magnetic field; it is usually lower than R_2 (Hashemi, Bradley, & Lisanti, 2012). The main applications of R_2 and R_1 are based on the relaxation behaviour of water protons (Mariette, 2009). Variations in R_2 and R_1 reflect changes in macromolecule concentration, water migration and structure in food matrices, but also environmental parameters, such as pH and temperature (Mariette, 2009; Peters et al., 2016). While this indicates the potential of R_2 and R_1 for monitoring digestive processes, many factors in play require careful validation of the meaning of R_2 and R_1 changes in different digestion contexts. As a first step, our recent study provided evidence that changes in R_2 can reflect protein hydrolysis of whey protein gels in a static *in vitro* digestion model (Deng, Janssen, et al., 2020). It is, however, unclear if relaxation rates can also be used to monitor protein digestion under dynamic circumstances, such as changing pH and protein concentration. To monitor these two variables during digestion, we hypothesised that it would be useful to include R_1 as an additional parameter. As such, we aimed to investigate the extent to which the combination of R_2 and R_1 measurements could be used to monitor digestion in a dynamic *in vitro* model, using whey protein gels as the model food.

To this end, we developed a novel MRI-compatible semi-dynamic Gastric Simulator (MR-GAS). In this model, we performed *in vitro* gastric digestion of whey protein gels in the laboratory and in a clinical MRI scanner. We quantified the degree of digestion and pH in the supernatant and measured its R_2 and R_1 with TD-NMR and MRI. Finally, the feasibility of R_2 and R_1 measurements to monitor pH and protein concentration under semi-dynamic gastric digestion conditions was evaluated by comparing the measured values and predictions.

2. Materials & methods

2.1. Materials

Pierce™ BCA Protein Assay Kit was purchased from Thermo Fisher Scientific, Inc. (Waltham, Massachusetts, USA). Pepsin from porcine gastric mucosa (541–623 activity units/mg), gastric mucin from porcine stomach and all other chemicals were purchased from Sigma Aldrich, Inc. (St. Louis, USA). Whey Protein Isolated (WPI) was purchased from Davisco Food International, Inc. (Le Sueur, USA). WPI has a protein content of 97.9 wt%, fat ≤ 1 wt%, ash ≤ 0.5 wt%, and lactose ≤ 0.5 wt% (percentages on dry matter basis). Milli-Q water (resistivity 18.2 M Ω cm at 25 °C, Merck Millipore, Billerica, USA) was used in all experiments.

2.2. Preparation of WPI gels

WPI gels were prepared as described previously (Deng, Janssen, et al., 2020). WPI was dissolved in water (15 wt% or 20 wt%) and stirred at room temperature for 2–3 h. No pH adjustments were done. The solutions were centrifuged at 1000 rpm for 10 min to eliminate air bubbles. Then the solutions were transferred to Teflon tubes and heated in a 90 °C water bath for 30 min. After that, the Teflon tubes were immediately cooled in an ice-water bath and then stored at 4 °C, 1–5 days prior to use. Before digestion experiments, the gels were cut into 5 mm diameter square particles with a gel cutter.

2.3. Preparation of simulated gastric fluid

Simulated gastric fluid (SGF) was prepared by dissolving NaCl (8.775 g/L), gastric mucin (1.5 g/L), pepsin (2000 activity units/mL) (Brodkorb et al., 2019; Kong & Singh, 2008). The initial pH of the SGF was adjusted to 1.5 using 2M HCl (Guo et al., 2015).

2.4. MR-GAS set-up

The MRI-compatible semi-dynamic gastric simulator (MR-GAS) set-

up is shown in Fig. 1. It consisted of a gastric secretion unit, a gastric empty unit, a stomach chamber, a water bath and tubing to deliver different flows. It is referred to as 'semi-dynamic' because it lacked stomach muscle contraction and the constant rates of gastric secretion and emptying that are *in vivo*, which are regulated by the nutrients density, digestion rate etc. The stomach chamber is a water-jacketed compartment of 500 mL heated to 37 °C by a circulating heater (Julabo GmbH, Germany). One of the main challenges for an MRI compatible digestion system is avoiding the use of metal. For gastric mixing, instead of magnetic stirrers, an airflow with a pressure of 0.2 bar was introduced to the bottom of the stomach chamber with a custom-built circular tubing with equally distributed holes. This was used to create air bubbles that mixed the food particles and SGF. To mimic gastric secretion, SGF, preheated to 37 °C in a container with water, was delivered to the stomach chamber via a syringe pump (NE-500 Programmable OEM Syringe Pump, New Era Pump Systems, Inc., USA) through a 5 mm (inner-diameter) PVC tube. Gastric content was emptied by a peristaltic pump (Watson Marlow, USA) through a 4 mm (inner-diameter) PVC tube. A sealed vessel with water was placed between the stomach chamber and the peristaltic pump to prevent emptied digesta from blocking the peristaltic pump tube.

2.5. *In vitro* gastric digestion in the MR-GAS

To initiate digestion, 50 g of the WPI gel particles were placed in the stomach chamber containing 150 mL of pre-heated SGF at 37 °C. Gastric secretion was immediately started at a rate of 2.5 mL/min and maintained throughout digestion. Gastric emptying was started 30 min after the start of digestion at a rate of 3.33 mL/min. The rates of gastric secretion and emptying were based on a digestion model reflecting normal adults (Guo et al., 2015).

2.6. Protein digestion measurements

To examine the extent of protein hydrolysis during digestion, we measured the free amino groups and protein concentration in the supernatant in the MR-GAS stomach chamber. At $t = 0, 5, 10, 15, 20, 30, 60, 90$ and 120 min after starting digestion, 1 mL supernatant samples were withdrawn from the stomach chamber. Each sample was placed in an Eppendorf tube containing sodium bicarbonate (0.015 g) and vortexed for 5 s to elevate pH to 8 and stop pepsin activity as recommended by Brodtkorb et al. (2019). After that, the concentration of released amino groups (-NH₂ groups) was measured with the OPA (*o*-phthalaldehyde) method, as described previously (Deng, Mars, Van Der Sman, Smeets, & Janssen, 2020). The protein concentration was measured by the BCA (Bicinchoninic Acid) method with the use of Pierce™ BCA Protein Assay Kit. The degree of hydrolysis (DH) was calculated with equation 1 - 5 in the Supplementary material.

During digestion, the pH of the supernatant was monitored with a pH meter (Metrohm Titrimo 877, Switzerland). The H⁺ balance was calculated with equation 6 - 11 in the Supplementary material.

2.7. TD-NMR measurements

At $t = 0, 15, 30, 60, 90$ and 120 min after starting digestion, 150 μL supernatant samples were collected from the stomach chamber and immediately (within 30 s) measured with TD-NMR as follows: Each sample was pipetted in a 7 mm NMR tube, and the tube was sealed to prevent water loss during the measurements. It was then placed in a Maran Ultra NMR spectrophotometer (Resonance Instruments Ltd., Witney, UK) to perform ¹H TD-NMR relaxometry at 0.72 T with the use of RINMR software (Resonance Instruments Ltd., Witney, UK).

T₂ was measured by the Carr-Purcell-Meiboom-Gill (CPMG) sequence (McIntosh, 2013). During the CPMG pulse train, 12,288 echoes (five data points per echo) were recorded with an echo time of 0.8 ms. Four transients were recorded with phase cycling, with a repetition time

of 15 s. Each echo in the CPMG echo train was phase-corrected and averaged to one data point by using an in-house routine programmed in IDL (ITT Visual Information Solutions, Boulder, CO, USA). The transverse magnetisation decay curves were analysed with a numerical inverse Laplace transform by CONTIN, and the distribution of amplitude at different T₂ values was established (Provencher & Vogel, 1983). From the distribution curve, average T₂ was acquired, and R₂ (=T₂⁻¹) values were calculated.

T₁ was measured by Continuous Wave Free Precession (CWFP-T₁) pulses with low flip angles (Morales, Monaretto, & Colnago, 2016). The first pulse was a 180° pulse, followed by a pause (T_p/2 = 125 μs) and a flip angle of ≈22° separated by T_p (250 μs). During the CWFP-T₁ pulse train, 32,768 echoes (two data points per echo) were recorded with an echo time of 0.5 ms. Four transients were recorded with phase cycling and a relaxation delay of 40 s. Each echo in the CWFP-T₁ echo train was phase-corrected, and each echo was averaged to one data point using an in-house IDL routine. Average T₁ was acquired and used to calculate average R₁ (=T₁⁻¹).

2.8. MRI measurements

For the MRI scans, the MR-GAS stomach chamber was placed in a 3T MRI scanner (Philips Ingenia Elition X, Philips Medical Systems, the Netherlands). A 16 channel small extremity coil was wrapped around the stomach chamber. MRI scans were conducted at baseline before adding protein gels and after digestion for 5, 15, 30, 45, 60 and 90 min. During each scan, the gastric secretion, gastric emptying, air mixing and the recirculating heater were switched off to reduce artefacts caused by motion/influx. For T₂ mapping, a 2D multi-echo spin-echo sequence was used (repetition time = 3000 ms, 32 echo times ranging from 60 to 2520 ms with an echo-spacing of 80 ms, matrix = 64 × 64, field of view (FOV) = 120 × 120 mm, in-plane resolution = 1.87 × 1.87 mm, 3.0 mm slice thickness, total acquisition time = 1 min 20 s).

For the image processing, the first echo time of 60 ms was removed to reduce systematic error and to achieve a better fit (Bonny, Zanca, Boire, & Veyre, 1996; Milford, Rosbach, Bendszus, & Heiland, 2015). T₂-maps were calculated based on the acquired images at 31 echo times using a Levenberg-Marquard two-parameter curve fitting in MATLAB R2018b (MathWorks, Natick, USA) with equation (1).

$$M_t = M_0 \cdot e^{-\frac{t}{T_2}} + offset \quad (1)$$

With t (echo time) and M_t , which is the voxel intensity at echo time t , we calculated the T₂ of each voxel, offset and M_0 (voxel equilibrium magnetic intensity).

For T₁ mapping, a 2D multi-echo GR/IR sequence was used (8 inversion times (TI) of 150, 570, 985, 1400, 1900, 2700, 4000 and 5000 ms, matrix = 64 × 64, FOV = 120 × 120 mm, in-plane resolution = 1.87 × 1.87 mm, 3.0 mm slice thickness, acquisition time 1-4 s per TI).

T₁-maps were calculated based on the acquired images at 8 inversion times using a Levenberg-Marquard two-parameter curve fitting in MATLAB R2018b (MathWorks, Natick, USA) using equation (2).

$$M_t = 1 - M_0 \cdot \left(1 - e^{-\frac{TI}{T_1}}\right) \quad (2)$$

With the inversion time (TI) and M_t , which is the voxel intensity at TI, we calculated M_0 (voxel equilibrium magnetic intensity) and T₁ for each voxel.

For each time point, the supernatant was segmented manually on both the T₁ and T₂ map with the use of the MIPAV software (Bazin et al., 2007) (Fig. S1 in Supplementary material). The mean T₁, R₁ (=T₁⁻¹), T₂ and R₂ (=T₂⁻¹) of the supernatant were calculated.

2.9. Statistical analysis

The means and standard deviations were calculated based on duplicates. In this paper, the expressions 'value ± value' represent 'mean ±

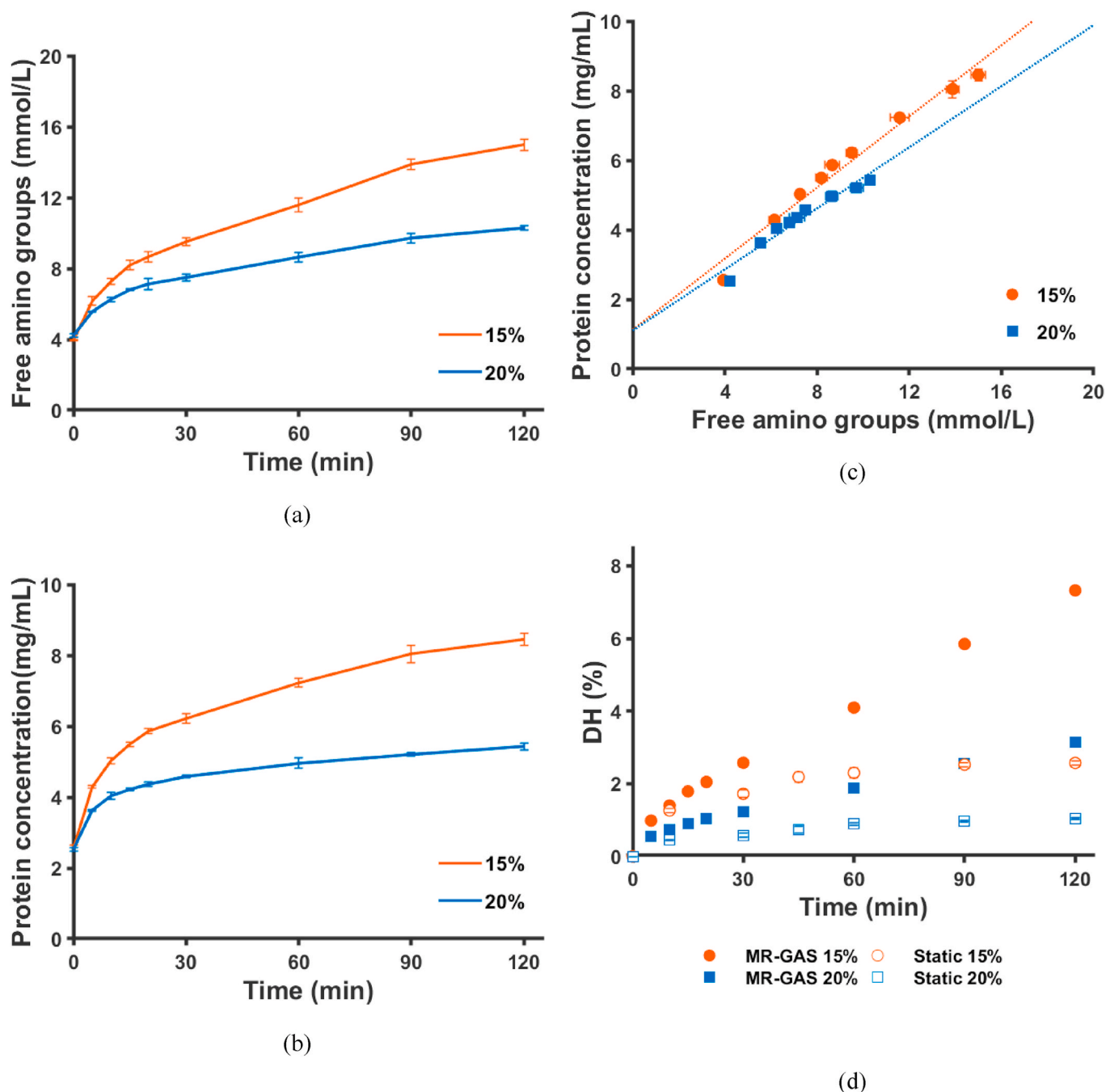


Fig. 2. Free amino groups (a), protein concentration (b), the linear correlation (with explained variance of 0.96 and 0.96) between protein concentration and free amino groups (c) in the supernatant during gastric digestion of 15% gel and 20% gel, and DH (d) of 15% gel and 20% gel in MR-GAS and a static digestion model (data from Deng, Janssen, et al. (2020)).

standard deviation'. In the figures, the error bars represent standard deviations. The regression analyses for R_2 and R_1 with protein concentration and $[H^+]$ were performed with the Curve Fitting Tool in Matlab R2018b (MathWorks, Natick, USA). To evaluate the goodness of prediction compared to the measured value, the normalised root mean squared deviation (NRMSD) was calculated with equation (3).

$$NRMSD = \frac{1}{\bar{y}^m} \cdot \sqrt{\frac{\sum_{i=1}^n (y_i^m - y_i^e)^2}{n}} \quad (3)$$

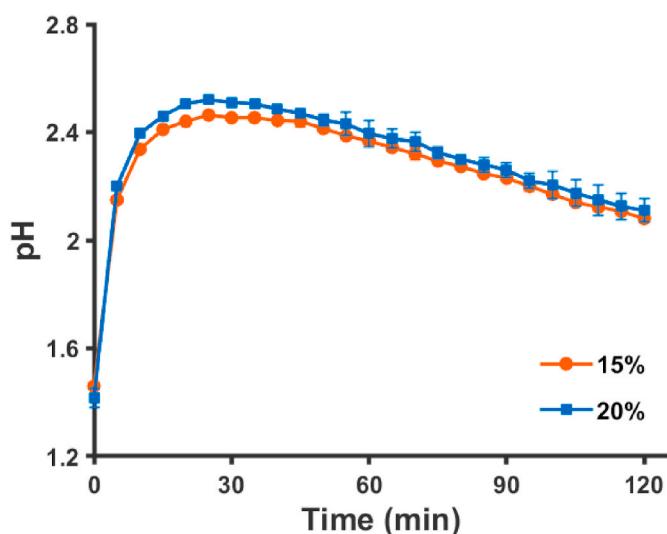
where \bar{y}^m is the mean of the measured values at all data points; y_i^m and y_i^e are the measured value and predicted value respectively at data point i ; n is the total amount of data points.

3. Results and discussion

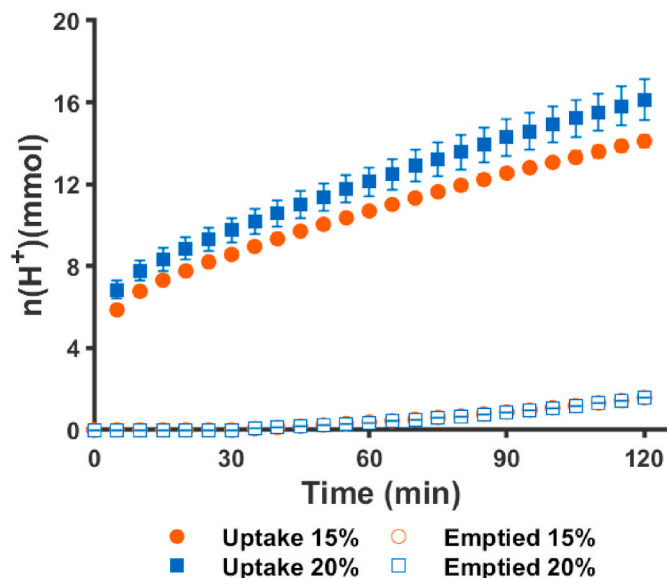
3.1. Digestion of protein gels in MR-GAS

The MR-GAS was set up and tested for the digestion of WPI gels under lab conditions. The concentration of free amino groups ($-NH_2$ groups, Fig. 2a) and protein concentration (Fig. 2b) in the supernatant showed the extent of protein digestion over time.

During the first 30 min of digestion, the concentration of $-NH_2$ groups increased by 5.57 ± 0.23 mM for the 15% WPI gel and by 3.28 ± 0.20 mM for the 20% gel. Throughout the rest of gastric digestion, the concentration of $-NH_2$ groups increased slower for both gels. As expected, the change in protein concentration was similar to that in $-NH_2$



(a)



(b)

Fig. 3. pH of the supernatant during gastric digestion of 15% gel and 20% gel (a) and the amount of acid uptake by the system and acid emptied of 15% gel and 20% gel during digestion (b).

groups: in the first 30 min, protein concentration of the 15% gel increased by 3.67 ± 0.13 and that of the 20% gel by 2.05 ± 0.04 mg/mL. The finding that protein gels were digested at a rapid rate in the first 30 min during the gastric phase is in line with previous studies (Deng, Janssen, et al., 2020; Luo, Boom, & Janssen, 2015). To mimic gastric emptying, the supernatant was removed from the stomach chamber after digestion for 30 min till the end. Therefore, the real-time peptide concentration in the supernatant (in Fig. 2a) does not represent the total amount of peptide produced. The total amount of peptide produced was calculated to obtain the degree of hydrolysis, which is discussed later. In line with other studies, the 15% gel was digested faster and to a larger extent than the 20% gel (Deng, Janssen, et al., 2020; Luo et al., 2015).

This is because the higher crosslinking density in 20% gel slows down the digestion via limiting pepsin diffusion, hydrolysis rate and microstructure transformation (Luo, Borst, Westphal, Boom, & Janssen, 2017).

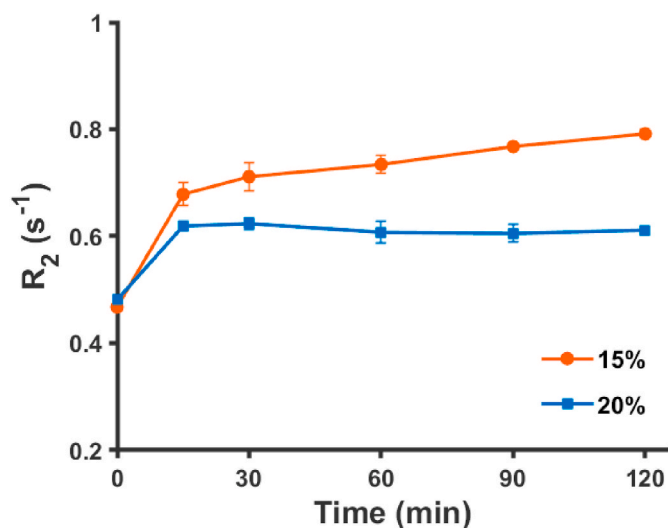
When protein concentration was plotted against the free amino acid group concentration in the supernatant, linear associations were observed for both gels (Fig. 2c). The slope of the 15% gel was higher than that of the 20% gel. This indicates that the average size of released peptides from both gels remains constant during digestion, and the average size of released peptides from the 20% gel was smaller compared to that from the 15% gel.

Compared to the results with a static model from Deng, Janssen, et al. (2020), the degree of hydrolysis (DH) of protein gels in the MR-GAS was much higher (Fig. 2d); after 2 h of digestion, DH of the 15% gel was 2.6% in the static model, whereas it was 7.3% in the MR-GAS. For the 20% gel, DH was 1.0% in the static model and 3.1% in the MR-GAS. A higher digestion rate in dynamic models is comparable with results from other studies (Egger et al., 2018; Mennah-Govela & Bornhorst, 2021; Miralles, del Barrio, Cueva, Recio, & Amigo, 2018). Interestingly, for both gels, the slope of the DH curves in the static model decreased after 1 h and the curves appear to nearly reach plateaus, while DH curves in the MR-GAS retained a rapid increase over 2 h. Digestion in another dynamic digestion model showed a similar trend of increased DH to our results with MR-GAS (Mennah-Govela & Bornhorst, 2021). The reason for the difference between static and (semi-)dynamic digestion in DH changes is that with a (semi-)dynamic model, there is a continuous supply of pepsin and acid. This (1) increases the enzyme to substrate ratio and (2) lowers the pH. Both accelerate the enzymatic hydrolysis. Compared to a static model, the higher digestion rate in the MR-GAS confirmed the importance of performing *in vitro* digestion experiments under (semi-)dynamic conditions.

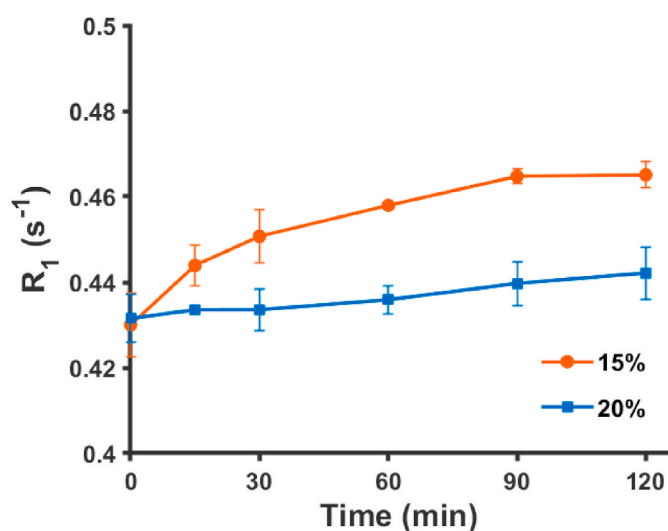
The pH of the supernatant was measured during the digestion of the 15% and 20% gels (Fig. 3a). The initial pH was 1.5. Within the first 15–30 min, the pH increased as a result of the buffering capacity of the gels and the released protein fraction from the gels to the supernatant (Deng, Mars, et al., 2020). After around 30 min, the pH of the supernatant decreased for both gels. It should be noted that SGF was continuously secreted throughout digestion, which decreased the pH, even though H^+ was taken up due to the buffering capacity and protein hydrolysis. Although the peptide concentration in the supernatant during digestion of the 20% gel was lower than that of the 15% gel, the pH in the supernatant of the 20% gel was higher than that of the 15% gel. This is likely due to the higher buffering capacity of the 20% gel. This is in accordance with another study in which protein gels with higher protein concentrations showed higher buffering capacity and a higher pH increase during gastric digestion (Luo, Zhan, Boom, & Janssen, 2018).

A mass balance of H^+ was set up, which included the gastric juice secretion, uptake of H^+ due to buffering capacity and protein hydrolysis, gastric emptying, and the net H^+ in the supernatant (Fig. S2 in Supplementary material). As shown in Fig. 3b, the majority of H^+ was taken up during digestion, as a sum result of buffering capacity and protein hydrolysis. The entire H^+ uptake of the 20% gel was higher than that of the 15% gel. After 2 h of digestion, acid uptake of the 15% gel was 1.9 mol/kg protein. This value is higher than that of the same gel in a static digestion model (1.6 mol/kg protein, Deng, Mars, et al., 2020), because of faster protein hydrolysis in the MR-GAS. Although we did not measure the amount of acid uptake without pepsin during the buffering reaction of our gel till pH 1.5, Mennah-Govela, Singh, and Bornhorst (2019) reported that it was 1.2 mol/kg protein for a 16% WPI gel. The curve also shows that after 2 h of digestion, equilibrium was not yet reached, which implies that the pH of protein gels may still be higher than that of the SGF and that digestion could still be progressing. This is in line with the increasing trend of the DH curve in Fig. 2d.

To summarise, similar to previous studies, the 15% gel digested faster than the 20% gel, and both gels digested faster in the MR-GAS



(a)



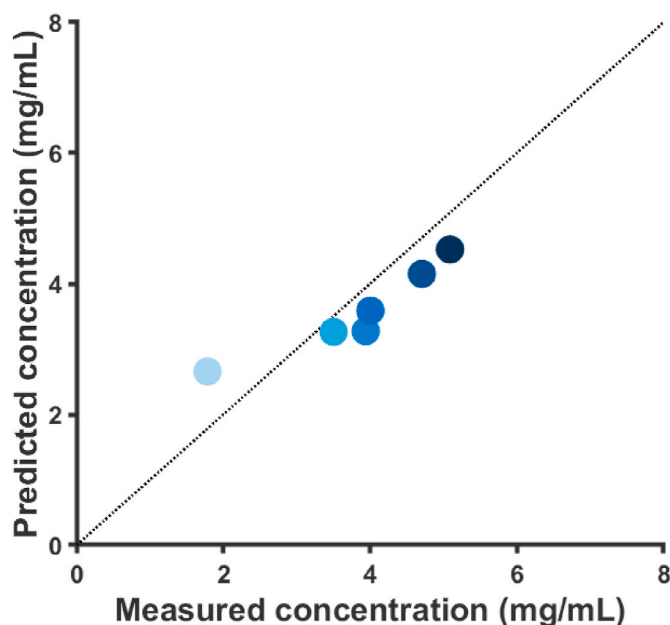
(b)

Fig. 4. R_2 (a) and R_1 (b) of supernatant during digestion of 15% gel and 20% gel, measured via TD-NMR.

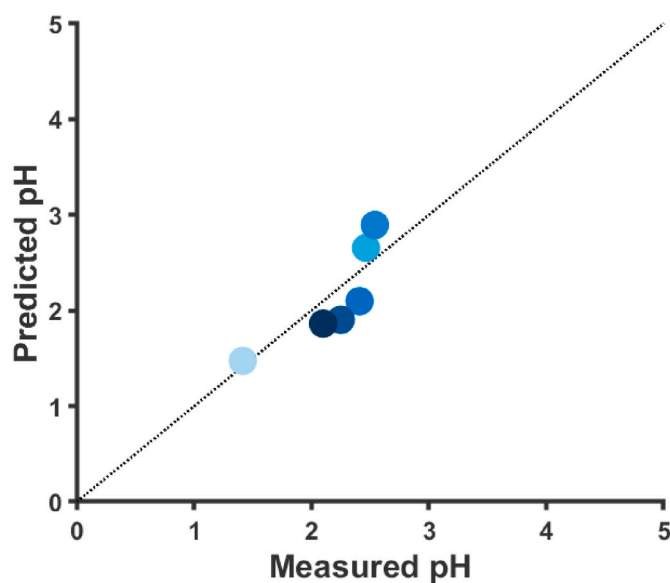
than in a static digestion model. The MR-GAS model has proven to be an adequate semi-dynamic digestion model. Remarkably, mixing of the gastric contents with the use of airflow was apparently effective and allowed the use of the stomach chamber within an MRI scanner.

3.2. R_2 and R_1 during digestion in MR-GAS

During the digestion of the 15% and the 20% gels in the MR-GAS, the supernatant was sampled, and transverse (R_2) and longitudinal (R_1) relaxation rates were measured by TD-NMR (Fig. 4). For both gels, R_2 increased over time and the fastest in the first 15 min (Fig. 4a). A faster and larger increase in R_2 was observed for the 15% gel compared to the 20% gel. It has been reported that R_2 can be linearly positively associated with protein concentration in solutions at the same pH (Le Dean, Mariette, & Marin, 2004). It has also been shown that a higher H^+ concentration (i.e. lower pH) and smaller molecular size decrease R_2 (Ozel, Aydin, Grunin, & Oztop, 2018). In the current work, the effect of molecular size on R_2 may be ignored since the average size of the



(a)



(b)

Fig. 5. Predicted against measured protein concentration (a) and predicted against measured pH (b) in the supernatant during digestion of 20% gel (Scatters with light to darker blue represent individual time points from 0 to 120 min). Predictions based on TD-NMR data. (For interpretation of the references to colour in this figure legend, the reader is referred to the Web version of this article.)

released protein fraction remained consistent during digestion (see section 3.1). Therefore, the increased R_2 over time is presumably due to the release of protein into the supernatant. Moreover, the rapid increase of pH (decrease of $[H^+]$) in the first 15 min likely contributes to the increased R_2 as well. The significantly slower increase in R_2 after 15 min may be due to the slower increase in protein concentration and the increase in $[H^+]$. In line with our previous findings (Deng, Janssen, et al., 2020), a faster and larger increase in R_2 was observed for the 15%

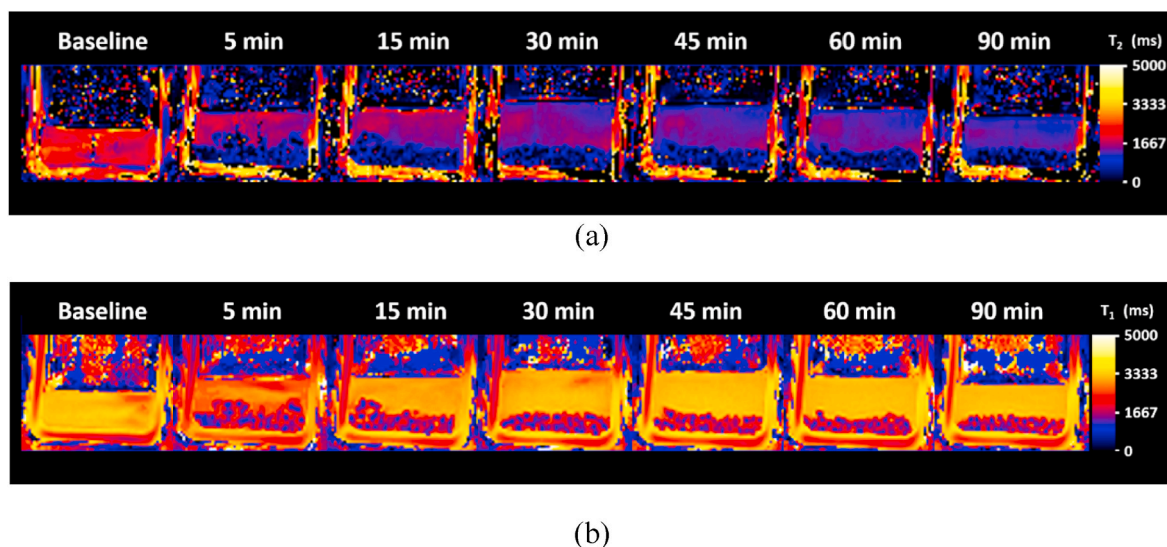


Fig. 6. T_2 maps (a) and T_1 maps (b) of the gastric content in MR-GAS during digestion of WPI 15% from baseline to 90 min ($T_2 = R_2^{-1}$ and $T_1 = R_1^{-1}$).

compared to the 20% gel, due to the faster digestion of the 15% gel.

Compared to R_2 , R_1 increased less during digestion (Fig. 4b). Similar to R_2 , higher protein concentration, lower $[H^+]$ and larger molecular size increase R_1 (Mariette, 2009; Oztop, Rosenberg, Rosenberg, McCarthy, & McCarthy, 2010). Therefore, in the current study, the increase in R_1 could be attributed not only to the increase in protein concentration but also to the steep decrease in $[H^+]$. Similar to R_2 , a faster and larger increase in R_1 was observed for the 15% compared to the 20% gel, because of a higher protein concentration in the supernatant. Compared to R_2 , R_1 showed less sensitivity to the changes in the protein concentration in the supernatant. In summary, both R_2 and R_1 increase during digestion and can therefore potentially serve as markers to track digestion.

3.3. Estimating protein concentration and pH with the use of R_2 and R_1

To check the feasibility of using R_2 and R_1 for monitoring digestion, we investigated the relationships between R_2 and R_1 with protein concentration and $[H^+]$ using data of the 15% gel and applied the obtained equations to predict the digestion of the 20% gel. Linear regression (Fig. S3 in Supplementary material) resulted in the following empirical equations and explained variance (R^2):

$$R_2 = 0.46 + 0.05 \cdot c_{\text{protein}} - 1.31 \cdot c_{\text{protein}} \cdot [H^+] \quad (R^2 = 0.99) \quad (4)$$

$$R_1 = 0.41 + 0.006 \cdot c_{\text{protein}} - 0.02 \cdot c_{\text{protein}} \cdot [H^+] \quad (R^2 = 0.96) \quad (5)$$

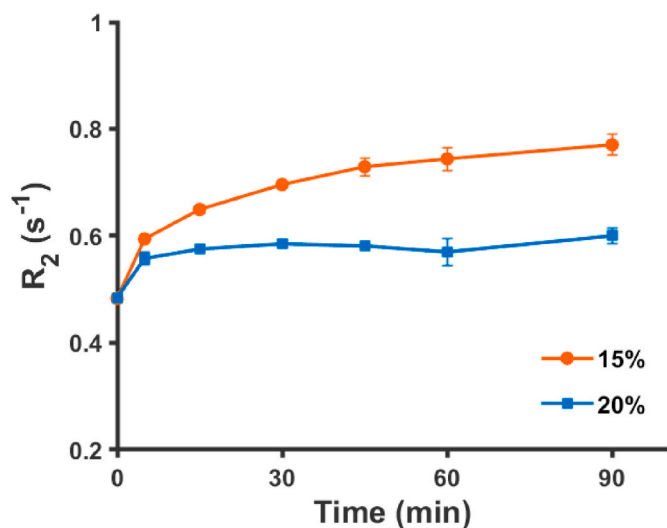
Using equations (4) and (5), we predicted the concentration of protein and H^+ in the supernatant during digestion of 20% gel and calculated the pH ($= -\log[H^+]$) and compared these predictions with the measured values as shown in Fig. 5. The normalised root mean squared deviation (NRMSD) was used to examine the goodness of prediction. An NRMSD of 0 indicates a perfect prediction. The NRMSD was 0.15 and 0.12 for the protein concentration and pH respectively. Thus, predicted protein concentration and pH were similar to the measured values. However, there was a small difference between the prediction and the measured values. This may be explained by the size of the released peptide from the 20% gel, which was slightly smaller than that from the 15% gel (see Section 3.1). This smaller molecular size results in a smaller relaxation rate. In summary, the results show that R_2 and R_1 can be effectively used as markers of changes in protein concentration and pH during *in vitro* gastric digestion of protein gels.

3.4. Monitoring digestion in the MR-GAS with MRI

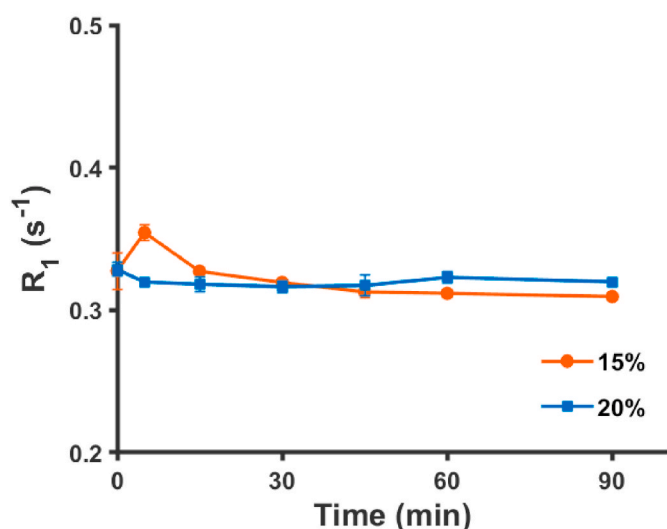
To further assess their potential for *in vivo* applications, R_2 and R_1 were measured by MRI during gastric digestion of 15% and 20% gels in the MR-GAS. While we only sampled supernatant in the TD-NMR measurements, with the MRI measurements, we measured both the gel and supernatant since the entire stomach chamber of the MR-GAS was placed in the MRI. Fig. 6 shows the colour-coded T_2 distribution and T_1 distribution in the stomach chamber during digestion of the 15% gel over time. In the baseline scan, there is only SGF present because that represents the fasting state. From $t = 5$ min onwards, two phases can be distinguished in the T_2 and T_1 maps, with protein gel particles visible in the lower part and the supernatant in the upper part. Fig. 7 shows the average R_2 and R_1 of the supernatant plotted against digestion time. The R_2 of the supernatant increased from 0.48 ± 0.001 to $0.77 \pm 0.02 \text{ s}^{-1}$ during 90 min of digestion (Fig. 7a), as was reflected in the change of colour from red to a darker blue in the T_2 map (Fig. 6a). This increase in R_2 was mainly caused by an increased protein concentration in the digesta. A smaller increase in R_2 was observed for the 20% gel because this gel was digested to a less extent. R_2 changes show a similar trend as that measured with TD-NMR (Fig. 4a), so we refer to the discussion in Section 3.2.

The R_1 of both the 15% and the 20% gels did not change much during digestion, except for an increase at $t = 5$ min for the 15% gel (Fig. 7b). The reason for this may be that R_1 is highly dependent on the magnetic field strength (Korb & Bryant, 2002). Since the MRI has a higher field strength (3T), it results in a smaller R_1 compared to that measured with TD-NMR (0.72 T). This could make the change in R_1 even smaller and harder to detect than with TD-NMR. The increase of R_1 at 5 min for the 15% gel was unexpected. Nelson and Tung (1987) showed that a lower temperature increases R_1 , and a stronger temperature effect was shown in the liquids with higher protein concentrations. Since, in our experiment, the SGF was heated to 37°C while the gel was at room temperature. The addition of the gel into the SGF resulted in a transient temperature decrease of approximately 5°C at $t = 5$ min. This could have caused the observed increase in R_1 . The higher protein concentration in the supernatant of the 15% gel may have reinforced this temperature effect compared to the 20% gel. However, more systematic research about how temperature affects the relaxation rates of acidic samples need to be conducted to support this explanation.

We determined the relationships between R_1 and R_2 with protein concentration and $[H^+]$ using data of the 15% gel and applied the obtained equation to predict the digestion of the 20% gel. Linear regression



(a)



(b)

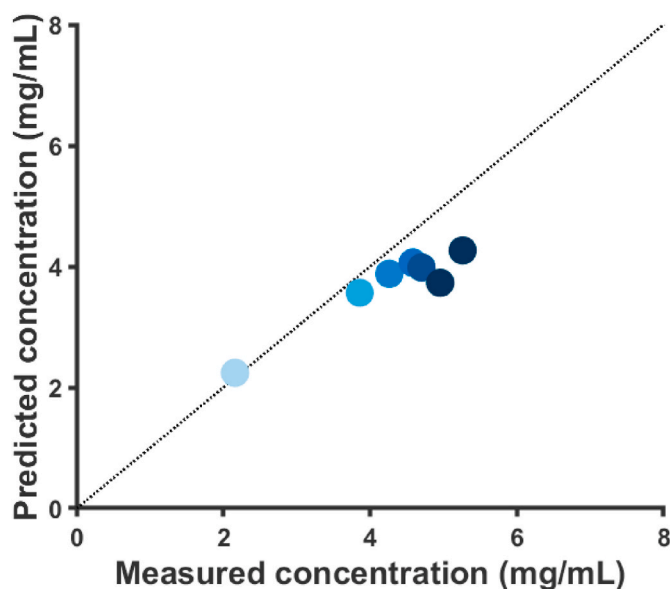
Fig. 7. R_2 (a) and R_1 (b) values of supernatant during 90 min digestion, measured via MRI.

(Fig. S4 in Supplementary material) resulted in the following empirical equations and explained variance (R^2):

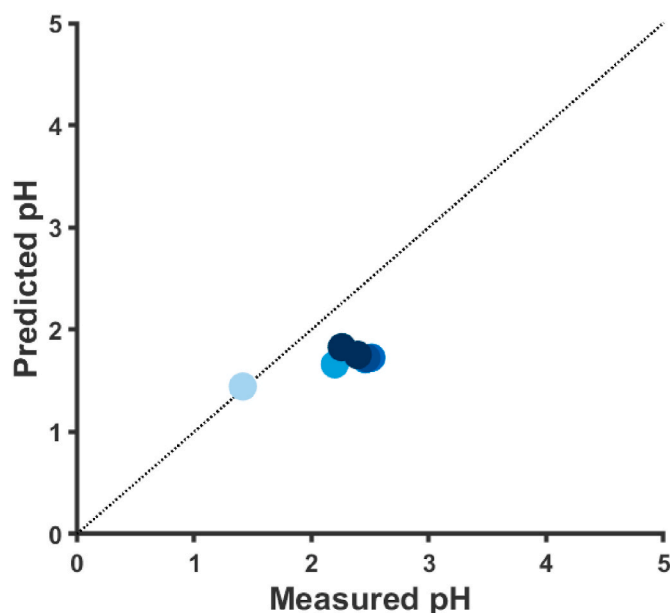
$$R_2 = 0.39 + 0.05 \cdot c_{protein} - 0.29 \cdot c_{protein} \cdot [H^+] \quad (R^2 = 0.99) \quad (6)$$

$$R_1 = 0.38 - 0.008 \cdot c_{protein} - 0.38 \cdot c_{protein} \cdot [H^+] \quad (R^2 = 0.60) \quad (7)$$

The lower explained variance in equation (7) was caused by the increase in R_1 at $t = 5$ min; omitting this data point increased the explained variance from 0.60 to 0.85. This is shown in Fig. S5 in Supplementary material. Using original equations (6) and (7) (without omitting $t = 5$ min), we predicted the protein concentration and $[H^+]$ in the supernatant during digestion of the 20% gel and calculated the pH ($= -\log[H^+]$). We compared the predictions with the measured values (Fig. 8). The NRMSD values were 0.18 and 0.29 for the protein concentration and pH respectively, and the values did not decrease, even when using the obtained equations that omitted $t = 5$ min (shown in Fig. S6 in Supplementary material). These NRMSD values were higher than those in the TD-NMR analysis. These less good predictions may be



(a)



(b)

Fig. 8. Predicted against measured protein concentration (a) and predicted against measured pH (b) in the supernatant during digestion of 20% gel (Scatters with light to darker blue represent individual time points from 0 to 120 min). Predictions based on MRI data. (For interpretation of the references to colour in this figure legend, the reader is referred to the Web version of this article.)

due to the fact that the R_1 (MRI) did not change much during digestion, so contributed less to the prediction. Thus, in this context, other magnetic resonance markers may be better suited as proxy measures for nutrient hydrolysis and pH change during digestion; however, they are currently underexplored (Smeets, Deng, van Eijnatten, & Mayar, 2020). The current results indicate that R_2 and R_1 are potential markers of protein concentration and acidic pH and may be used to monitor the semi-dynamic gastric digestion of protein gels in a clinical MRI. Such *in vitro* results can contribute to the interpretation of similar measures

done *in vivo*.

Based on the current study, the applications of MR-GAS can be further extended, including altering the rate of gastric secretion and emptying to mimic different gastric responses to different stages of gastric digestion, to different types of food or to represent different populations. Furthermore, it would be worthwhile exploring the application of the MR parameters to study digestion of other more complex food matrices and using a naturalistic pH trajectory.

4. Conclusion

In this study, we developed the MR-GAS: the first semi-dynamic MRI compatible *in vitro* gastric digestion model. The results demonstrate its capability to incorporate gastric secretion, emptying and mixing not only in a lab set-up, but also in a clinical MRI scanner. The protein digestion rate in the MR-GAS is comparable with that reported for other semi-dynamic models. Furthermore, we show that R_2 and R_1 , as measured with NMR and MRI, can be used to monitor digestion under dynamic circumstances: protein concentration and pH were the two main parameters that changed in the supernatant during digestion and the relationships between them with R_2 and R_1 were analysed with linear regression. Therefore, using the empirical equations obtained from the linear regression analysis, we were able to predict the protein concentration and pH with the input of measured R_2 and R_1 . Prediction with the use of R_2 and R_1 from TD-NMR was more accurate than that from MRI. Further research on MRI derived R_2 and R_1 measurements will be essential to bring *in vitro* results and *in vivo* data together, and the MR-GAS model can contribute to this translation. In conclusion, the MR-GAS is a useful tool for *in vitro* digestion MRI research and R_2 and R_1 could serve as markers of changes in protein concentration and pH during digestion. These findings set the stage for monitoring gastric protein digestion *in vivo* using MRI in the future.

Author statement

Ruoxuan Deng: Conceptualization, Methodology, Formal analysis, Investigation, Data curation, Visualization, Validation, Writing – original draft; Aurimas Seimys: Investigation, Methodology, Formal analysis, Writing – review; Monica Mars, Anja Janssen and Paul Smeets: Conceptualization, Methodology, Validation, Writing – review & editing, Supervision.

Declaration of competing interest

The authors declare no conflict of interest.

Acknowledgements

This work was supported by a China Scholarship Council grant. The use of the 3T MRI facility has been made possible by Wageningen University & Research Shared Research Facilities. The authors would like to thank Paul de Bruin for his support on the MRI sequences, Frank J. Vergeldt for his help with the TD-NMR T1 sequence, Henk Van As for the initial idea of using air bubbles for mixing and Jos Sewalt for the help with the MR-GAS set-up.

Appendix A. Supplementary data

Supplementary data to this article can be found online at <https://doi.org/10.1016/j.foodhyd.2021.107393>.

References

Bazin, P. L., Cuzzocreo, J. L., Yassa, M. A., Gandler, W., McAuliffe, M. J., Bassett, S. S., et al. (2007). Volumetric neuroimage analysis extensions for the MIPAV software package. *Journal of Neuroscience Methods*, 165(1), 111–121. <https://doi.org/10.1016/j.jneumeth.2007.05.024>

Bonny, J. M., Zanca, M., Boire, J. Y., & Veyre, A. (1996). T2 maximum likelihood estimation from multiple spin-echo magnitude images. *Magnetic Resonance in Medicine*. <https://doi.org/10.1002/mrm.1910360216>.

Bordoni, A., Picone, G., Babini, E., Vignali, M., Danesi, F., Valli, V., et al. (2011). NMR comparison of *in vitro* digestion of Parmigiano Reggiano cheese aged 15 and 30 months. *Magnetic Resonance in Chemistry*, 49(SUPPL. 1). <https://doi.org/10.1002/mrc.2847>

Bornhorst, G. M. (2017). Gastric mixing during food digestion: Mechanisms and applications. *Annual Review of Food Science and Technology*, 8(1), 523–542. <https://doi.org/10.1146/annurev-food-030216-025802>

Brodtkorb, A., Egger, L., Alminger, M., Alvito, P., Assunção, R., Ballance, S., et al. (2019). INFOGEST static *in vitro* simulation of gastrointestinal food digestion. *Nature Protocols*, 14(4), 991–1014. <https://doi.org/10.1038/s41596-018-0119-1>

Deng, R., Janssen, A. E. M., Vergeldt, F. J., Van As, H., de Graaf, C., Mars, M., et al. (2020). Exploring *in vitro* gastric digestion of whey protein by time-domain nuclear magnetic resonance and magnetic resonance imaging. *Food Hydrocolloids*, 99, 105348. <https://doi.org/10.1016/j.foodhyd.2019.105348>

Deng, R., Mars, M., Van Der Sman, R. G. M., Smeets, P. A. M., & Janssen, A. E. M. (2020). The importance of swelling for *in vitro* gastric digestion of whey protein gels. *Food Chemistry*, 330, 127182. <https://doi.org/10.1016/j.foodchem.2020.127182>

Egger, L., Ménard, O., Baumann, C., Duerr, D., Schlegel, P., Stoll, P., et al. (2018). Digestion of milk proteins: Comparing static and dynamic *in vitro* digestion systems with *in vivo* data. *Food Research International*. <https://doi.org/10.1016/j.foodres.2017.12.049> (October), 0–1.

Gouseti, O., Bornhorst, G. M., Bakalis, S., & Mackie, A. (2019). In O. Gouseti, G. M. Bornhorst, S. Bakalis, & A. Mackie (Eds.), *Interdisciplinary approaches to food digestion: Interdisciplinary approaches to food digestion*. Cham: Springer International Publishing. <https://doi.org/10.1007/978-3-030-03901-1>.

Guo, Q., Ye, A., Lad, M., Ferrua, M., Dalgleish, D., & Singh, H. (2015). Disintegration kinetics of food gels during gastric digestion and its role on gastric emptying: An *in vitro* analysis. *Food and Function*, 6(3), 756–764. <https://doi.org/10.1039/c4fo00700j>

Hashemi, R. H., Bradley, W. G., & Lisanti, C. J. (2012). *MRI: The basics: The basics*. Lippincott Williams & Wilkins.

Kong, F., & Singh, R. P. (2008). A model stomach system to investigate disintegration kinetics of solid foods during gastric digestion. *Journal of Food Science*, 73(5), 202–210. <https://doi.org/10.1111/j.1750-3841.2008.00745.x>

Korb, J. P., & Bryant, R. G. (2002). Magnetic field dependence of proton spin-lattice relaxation times. *Magnetic resonance in medicine*. <https://doi.org/10.1002/mrm.10185>

Le Dean, A., Mariette, F., & Marin, M. (2004). 1H nuclear magnetic resonance relaxometry study of water state in milk protein mixtures. *Journal of Agricultural and Food Chemistry*, 52(17), 5449–5455. <https://doi.org/10.1021/jf030777m>

Luo, Q., Boom, R. M., & Janssen, A. E. M. (2015). Digestion of protein and protein gels in simulated gastric environment. *Lebensmittel-Wissenschaft und -Technologie- Food Science and Technology*, 63(1), 161–168. <https://doi.org/10.1016/j.lwt.2015.03.087>

Luo, Q., Borst, J. W., Westphal, A. H., Boom, R. M., & Janssen, A. E. M. (2017). Pepsin diffusivity in whey protein gels and its effect on gastric digestion. *Food Hydrocolloids*, 66, 318–325. <https://doi.org/10.1016/j.foodhyd.2016.11.046>

Luo, Q., Zhan, W., Boom, R. M., & Janssen, A. E. M. (2018). Interactions between acid and proteins under *in vitro* gastric condition—a theoretical and experimental quantification. *Food and Function*, 9(10), 5283–5289. <https://doi.org/10.1039/c8fo01033a>

Marciani, L. (2011). Assessment of gastrointestinal motor functions by MRI: A comprehensive review. *Neuro-Gastroenterology and Motility*, 23(5), 399–407. <https://doi.org/10.1111/j.1365-2982.2011.01670.x>

Mariette, F. (2009). Investigations of food colloids by NMR and MRI. *Current Opinion in Colloid & Interface Science*, 14(3), 203–211. <https://doi.org/10.1016/j.cocis.2008.10.006>

McIntosh L, P. (2013). CPMG. In G. C. K. Roberts (Ed.), *Encyclopedia of biophysics* (p. 386). Berlin, Heidelberg: Springer Berlin Heidelberg. https://doi.org/10.1007/978-3-642-16712-6_320.

Mennah-Govela, Y. A., & Bornhorst, G. M. (2021). Breakdown mechanisms of whey protein gels during dynamic *in vitro* gastric digestion. *Food and function*. <https://doi.org/10.1039/d0fo03325a>

Mennah-Govela, Y. A., Singh, R. P., & Bornhorst, G. M. (2019). Buffering capacity of protein-based model food systems in the context of gastric digestion. *Food & Function*, 10(9), 6074–6087. <https://doi.org/10.1039/C9FO01160A>

Milford, D., Rosbach, N., Bendszus, M., & Heiland, S. (2015). Mono-exponential fitting in T2-relaxometry: Relevance of offset and first echo. *PLoS One*. <https://doi.org/10.1371/journal.pone.0145255>

Minekus, M., Alminger, M., Alvito, P., Ballance, S., Bohn, T., Bourliou, C., et al. (2014). A standardised static *in vitro* digestion method suitable for food—an international consensus. *Food and Function*, 5(6), 1113–1124. <https://doi.org/10.1039/c3fo60702j>

Miralles, B., del Barrio, R., Cueva, C., Recio, I., & Amigo, L. (2018). Dynamic gastric digestion of a commercial whey protein concentrate. *Journal of the Science of Food and Agriculture*, 98(5), 1873–1879. <https://doi.org/10.1002/jsfa.8668>

Moraes, T. B., Monaretto, T., & Colnago, L. A. (2016). Rapid and simple determination of T1 relaxation times in time-domain NMR by Continuous Wave Free Precession sequence. *Journal of Magnetic Resonance*, 270, 1–6. <https://doi.org/10.1016/j.jmr.2016.06.019>

Nelson, T. R., & Tung, S. M. (1987). Temperature dependence of proton relaxation times *in vitro*. *Magnetic Resonance Imaging*, 5(3), 189–199. [https://doi.org/10.1016/0730-725X\(87\)90020-8](https://doi.org/10.1016/0730-725X(87)90020-8)

- Ozel, B., Aydin, O., Grunin, L., & Oztop, M. H. (2018). Physico-chemical changes of composite whey protein hydrogels in simulated gastric fluid conditions. *Journal of Agricultural and Food Chemistry*, 66(36), 9542–9555. <https://doi.org/10.1021/acs.jafc.8b02829>. research-article.
- Oztop, M. H., Rosenberg, M., Rosenberg, Y., McCarthy, K. L., & McCarthy, M. J. (2010). Magnetic resonance imaging (MRI) and relaxation spectrum analysis as methods to investigate swelling in whey protein gels. *Journal of Food Science*, 75(8). <https://doi.org/10.1111/j.1750-3841.2010.01788.x>
- Peters, J. P. C. M., Vergeldt, F. J., Van As, H., Luyten, H., Boom, R. M., & van der Goot, A. J. (2016). Time domain nuclear magnetic resonance as a method to determine and characterize the water-binding capacity of whey protein microparticles. *Food Hydrocolloids*, 54, 170–178. <https://doi.org/10.1016/j.foodhyd.2015.09.031>
- Singh, H., & Gallier, S. (2014). Processing of food structures in the gastrointestinal tract and physiological responses. Food structures, digestion and health. <https://doi.org/10.1016/B978-0-12-404610-8.00002-5>.
- Smeets, P. A. M., Deng, R., van Eijnatten, E. J. M., & Mayar, M. (2020). Monitoring food digestion with magnetic resonance techniques. *Proceedings of the Nutrition Society*, 1–11. <https://doi.org/10.1017/S0029665120007867>
- Spiller, R., & Marciani, L. (2019). Intraluminal impact of food: New insights from MRI. *Nutrients*, 11(5), 1147. <https://doi.org/10.3390/nu11051147>